IRAN : Interferometric Remapped Array Nulling

E. Aristidi[a], F. Vakili[a], L. Abe[a], A. Belu[a], B. Lopez[b], H. Lantéri[a], A. Schutz[a] and J.L. Menut[b]

[a]Laboratoire Univ. d'Astroph. de Nice (LUAN), CNRS UMR 6525, Parc Valrose, 06108 Nice Cedex 02, France;

[b]Laboratoire Fresnel, CNRS UMR 6528, Observatoire de la Côte d'Azur, B.P. 4229, 06304 Nice cedex 4

ABSTRACT

This paper describes a method of beam-combination in the so-called hypertelescope imaging technique recently introduced by Labeyrie in optical interferometry. The method we propose is an alternative to the Michelson pupil reconfiguration that suffers from the loss of the classical object-image convolution relation. From elementary theory of Fourier optics we demonstrate that this problem can be solved by observing in a combined pupil plane instead of an image plane. The point-source intensity distribution (PSID) of this interferometric "image" tends towards a pseudo Airy disc (similar to that of a giant monolithic telescope) for a sufficiently large number of telescopes. Our method is applicable to snap-shot imaging of extended sources with a field comparable to the Airy pattern of single telescopes operated in a co-phased multi-aperture interferometric array. It thus allows to apply conveniently pupil plane coronagraphy. Our technique called Interferometric Remapped Array Nulling (IRAN) is particularly suitable for high dynamic imaging of extra-solar planetary companions, circumstellar nebulosities or extra-galactic objects where long baseline interferometry would closely probe the central regions of AGNs for instance.

Keywords: Techniques: high angular resolution – Techniques: interferometry – Techniques: imaging

1. INTRODUCTION

The concept of densified pupil-hypertelescope introduced by Labeyrie[8] is a generalization of the classical Michelson periscopic set-up for stellar interferometry.[12] The principle is to increase the relative pupil size of individual telescopes (output pupil diameters normalized to the baselines) composing the interferometer, to fill up the disc of the equivalent single dish telescope. This non linear process modifies the classical object-image convolution relation for extended sources larger than the Airy discs of individual telescopes. Thus the non-aberrated imaging field of view can dramatically decrease with increasing so-called densification factor γ.[7]

We recently proposed a multiaxial pupil-plane imaging technique[16] which is equivalent to Labeyrie's hypertelescope technique with the extra bonus of conserving the convolution relation over a field limited to the super-imposed pupilla of the primary telescopes. Images this way formed in the pupil plane are similar to what can be expected at the focus of the giant equivalent telescope, excepted that the field is spatially limited by the geometrical image of the telescope pupils. This property is interesting in particular for exoplanet (ExPN) observations: compared to coaxial Bracewell nulling interferometry,[4] our concept presents the advantage of separating the ExPN energy from the zodiacal emission of its parent star. The paper is organised as follows. In section 2 we give the general formalism for object-image relation. In section 3 we focus on stellar companions detection and propose an apodisation technique for reducing the main star PSID secondary peaks. In section 4 we propose a deconvolution method for extended objects. Finally, in section 5 we discuss the combination of the interferometer with a AIC-type nuller[6] to perform high-dynamic exoplanet detection.

2. PRINCIPLE OF IRAN

Labeyrie's hypertelescope concept[8] is based on densifying the output pupil of an interferometric array by conserving the primary telescope orientations respective to each other to form the equivalent of a single dish telescope with a continuous surface. This is obtained for instance by re-imaging the output pupils on a pyramidal beam combiner.[7] The resulting diffraction pattern is formed by coherent addition of tilted Airy discs of individual telescopes. It exhibits a complicated fringe modulated image which tends to the Airy disc of the pseudo-densified

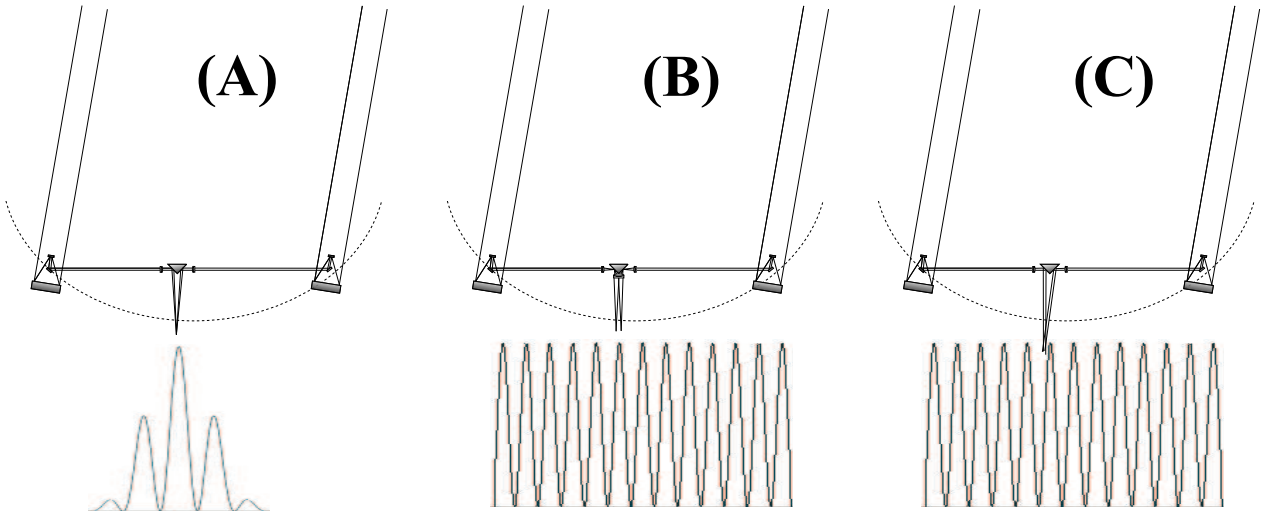

Figure 1. Generic comparison of three different beam-combinations for an optical stellar interferometer. (A) the classical Michelson beam-combination, (B) IRAN^a: instead of superimposing the Airy patterns from the telescopes it is possible to use a relay lens after the beam-combiner to stack the two output pupils on the top of each other with a modulation depending on the output Airy discs distance. (C) IRAN^b: pyramidal mirror gives small tilts (proportionnal to the telescope positions) to make the beams intersect. Output pupil are formed at this intersection.This pupil-plane interferometry can indeed be generalized to N telescopes described as IRAN beam-combination described in section 2.2.

aperture, thus resembling to a monolithic giant dish Airy pattern. In the IRAN concept beam-combination is simply obtained by forming tilted output pupils on the top of each other and record their interference on a 2D detector. The tilt given to each pupil is proportionnal to the position of the telescopes on the ground. As discussed hereafter, this can be achieved by forming an intermediate image plane and using a lens to form the interferometric pupil plane. Or by tilting the collimated beams from each telescope so that they intersect and use lenses to form a geometric image of the pupil at the intersection.

2.1. Technical implementation

To better understand the operating principle of IRAN it is useful to recall Michelson optical set-up for stellar interferometry (Fig. 1A). Output pupils forms on a pyramidal mirror, a relay lens produces the interferometric image. The fringe modulation does not depend on the spacing between the input telescope pupil size but on the output pupils as seen from the focal superimposed Airy patterns. In the Michelson set-up the basic convolution relation between the Point Spread Function and the object intensity distribution on the sky is lost (excepted if the object is small compared to the diffraction limit of individual telescopes) making image reconstruction from the measure of the complex visibility function mandatory. The fringe intensity pattern is modulated by the Airy envelope.

The Michelson set-up can be further modified[5] to form the Airy discs on the faces of the beam-combination mirror followed by a relay lens (Fig. 1B) which would form two superimposed and cosine-modulated output pupils where the fringe period depends on the Airy disc pattern distance as seen from the two superimposed pupils. We name IRAN^a this set-up. A modified version, denoted IRAN^b is presented in Fig. 1C, and gives the same interferometric pattern. The pyramidal mirror of the recombinator is shaped to give small tilts on the incident beams. Geometric tilted images of individual pupils intersect to form the interferogram.

In both cases the fringe modulation remains constant across the support of the superimposed pupils. Now if much more than two beams were remapped from a large number of input mirror segments the different period and orientation of the resulting cosine fringe modulations will produce a central bright spot at the center of the conjugate stacked pupil for an on-axis star.

Two beam-combination schemes could be envisaged in this case: a classical bulky optical pyramidal shape mirror[13] which generalizes (Fig. 1C) set-up versus a fiber optics (F.O.) beam combiner[11] with the bonus of modal

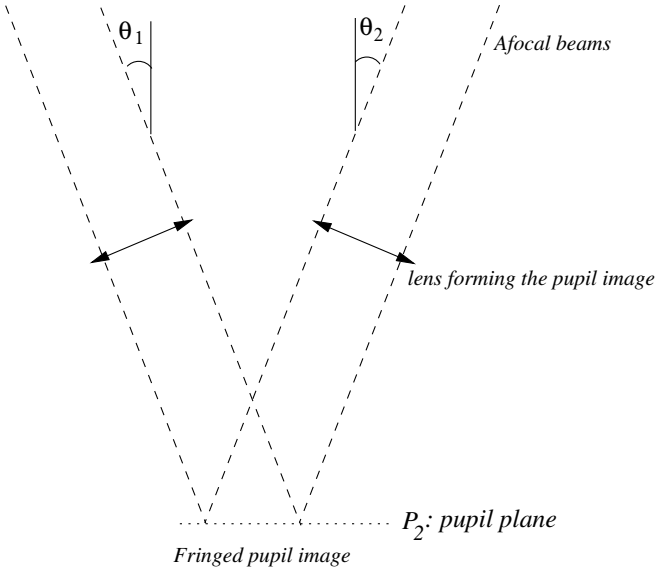

Figure 2. Optical layout of the IRAN^b beam-combiner. Collimated beams are coming from the telescopes with tilt angle $\vec{\theta}_i$. A lens forms a geometrical image of the pupil in the plane P_2 with a magnification γ. As all the beams cross in P_2, a fringed pupil image is observed.

filtering and an expected simplified beam-combiner. In the case of F.O. combination, the field of view would be limited to the Airy angular size of individual telescopes.

2.2. Intensity distribution for an on axis point-source

For sake of simplicity we consider a flat array of optical telescopes spread over co-centric rings with increasing radii and number of telescopes per ring. The telescopes afocal beams feed a central beam-combiner (Fig. 1C) after correction of the optical paths differences (OPD) between the telescopes. Here we develop the formalism for the IRAN^b combiner, the case of IRAN^a has been already written.[16] We will also consider a classical bulky optics recombinator (no fibers).

Let $\vec{R}_i$ the positions of the N telescopes on the ground. These telescopes are supposed identical, with diameter d_0 and focal length f_0. We suppose that the incoming light is monochromatic with a wavelength of λ.

Beam-collection from the N telescopes of the array is done at the intersection (plane P_2), where individual geometric pupil images are formed by relay lenses. A pyramidal mirror with N reflecting faces give to the beams a tilt proportionnal to the telescope position, so that the geometry is conserved.

We denote as $\vec{\theta}_i$ the tilt given to the beam number i. We have $\vec{\theta}_i = \eta\, \vec{R}_i$. We denote as χ the scaling factor of individual pupils, so that their diameter in the recombination plane is χd_0.

As in the previous paper,[16] we choosed to illustrate a telescope configuration distributed over 3 rings of diameters D_1, $D_2 = 2.4D_1$ and $D_3 = 3.8D_1$. 7 telescopes are equally distributed on the first ring, 13 on the second one and 19 on the third one. This configuration is non-redundant in order to minimize the energy spread in the secondary peaks of the PSID. All the figures shown hereafter, except section 5 about coronography, correspond to numerical simulations made with the configuration which follows: Wavelength $\lambda = 10\mu$m, diameter of the rings : $D_1 = 20$ m, $D_2 = 48$ m, $D_3 = 76$ m, telescope diameter d_0=1 m, scaling factor χ=0.03 so that the output pupil diameter is 3 cm, $\eta = 10^{-4}$ so that the tilt angle is 0.11°, 0.28° and 0.44° for beams coming from telescopes on the inner, medium and outer ring respectively

The intensity in the plane P_2 is given by

$$I_2(\vec{r}) = |P(\vec{r})|^2 \; . \; \left| \sum_{i=1}^{N} \exp -\frac{2i\pi\eta\vec{r}.\vec{R}_i}{\lambda} \right|^2 \qquad (1)$$

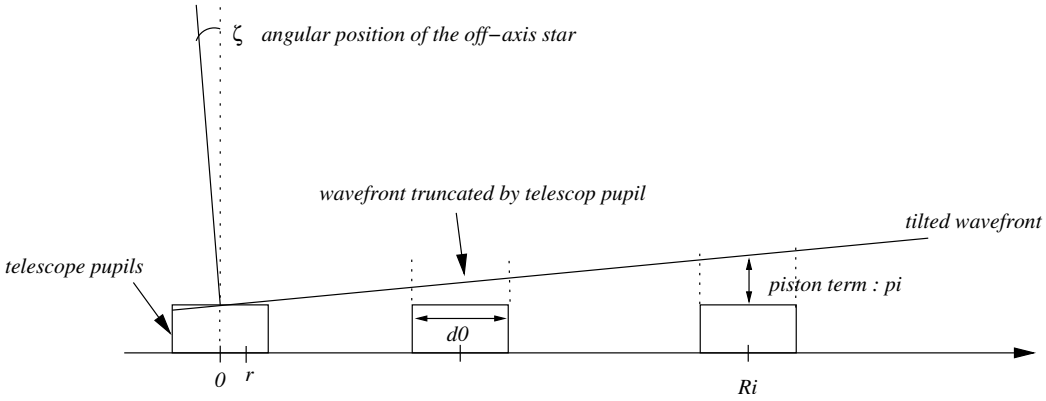

Figure 3. Simulated observation of an off-axis point-source at a distance ζ from the center of the field of view. On this one-dimensionnal configuration, each telescope is at a position R_i. The corresponding complex amplitude on each pupil is the product of a piston term $\exp 2i\pi\zeta R_i/\lambda$ by a tilt term $\exp 2i\pi\zeta r/\lambda$, r being the coordinate inside the pupil function.

where $P(\vec{r})$ is re-imaged telescope pupil, ideally a uniform disc of diameter χd_0. We can denote as $I_0(\vec{r}) = \left|\sum_{i=1}^{N} \exp -\frac{2i\pi\eta\vec{r}.\vec{R}_i}{\lambda}\right|^2$ the fringe term depending on the tilts.

This relation is equivalent to eq.4 of (Vakili et al., 2004)[16] that describes the formalism for IRAN[a] (with the transformation $\eta = 1/\gamma f_2$). Therefore the shape of the PSID is the same in both cases: it exhibits a central pseudo Airy disc surrounded by a "clean zone" with Airy rings, then a "dirty zone" with speckle-like residuals (coming from the gaps in uv coverage). The pattern is spatially limited by the achromatic pupil function $P(r)$. Fig. 4 gives illustrations in monochromatic/polychromatic light. As we will show hereafter, a pseudo-convolution relation applies between the source and its image, allowing to convert the scale in arcsec on the sky. Therefore, the pupil function will constitute the physical limit of the field of view (FOV) of the interferometer. Using eq. 5 this FOV is equal to $\eta\chi d_0$ in arcsec (0.6 arcsec for our simulation). Also, the diameter of the clean zone appears to be the angular resolution of a telescope of diameter D_1 (inner ring). Finally, the diameter of the central spot is the angular resolution of the interferometer.

2.3. The response for an off-axis point-source

We observe an off-axis point source of intensity O_0 in the direction given by the vector $\vec{\zeta} = (\alpha, \delta)$ where α (resp. δ) is the offset in right ascension (resp. declination, see fig. 3 for illustration). The incident flat wavefront is tilted with an angle $\vec{\zeta}$. This wavefront is sampled by the N-apertures pupil. For each sub-pupil, the products of two terms appear in the complex amplitude on the pupil: a piston term depending on the telescopes position

$$p_i = \exp \frac{2i\pi\vec{\zeta}.\vec{R}_i}{\lambda} \tag{2}$$

and a tilt term

$$t = \exp \frac{2i\pi\vec{\zeta}.\vec{r}}{\lambda} \tag{3}$$

where $\vec{r}$ is a position on the single telescope pupil. These terms will be conserved in the output pupils in the interferometric plane P_2. Note that the tilt term t is independent of the telescope, and can be included in the pupil function $P(r)$; it will indeed vanish in the intensity distribution where the square modulus of $P(r)$ appears.

Using the same formalism as (Vakili et al. 2004),[16] the intensity in the combined pupil plane P_2 expresses as

$$I_2(\vec{r}) = O_0|P(\vec{r})|^2 \,.\, I_0\left(\vec{r} - \frac{\vec{\zeta}}{\eta}\right) \tag{4}$$

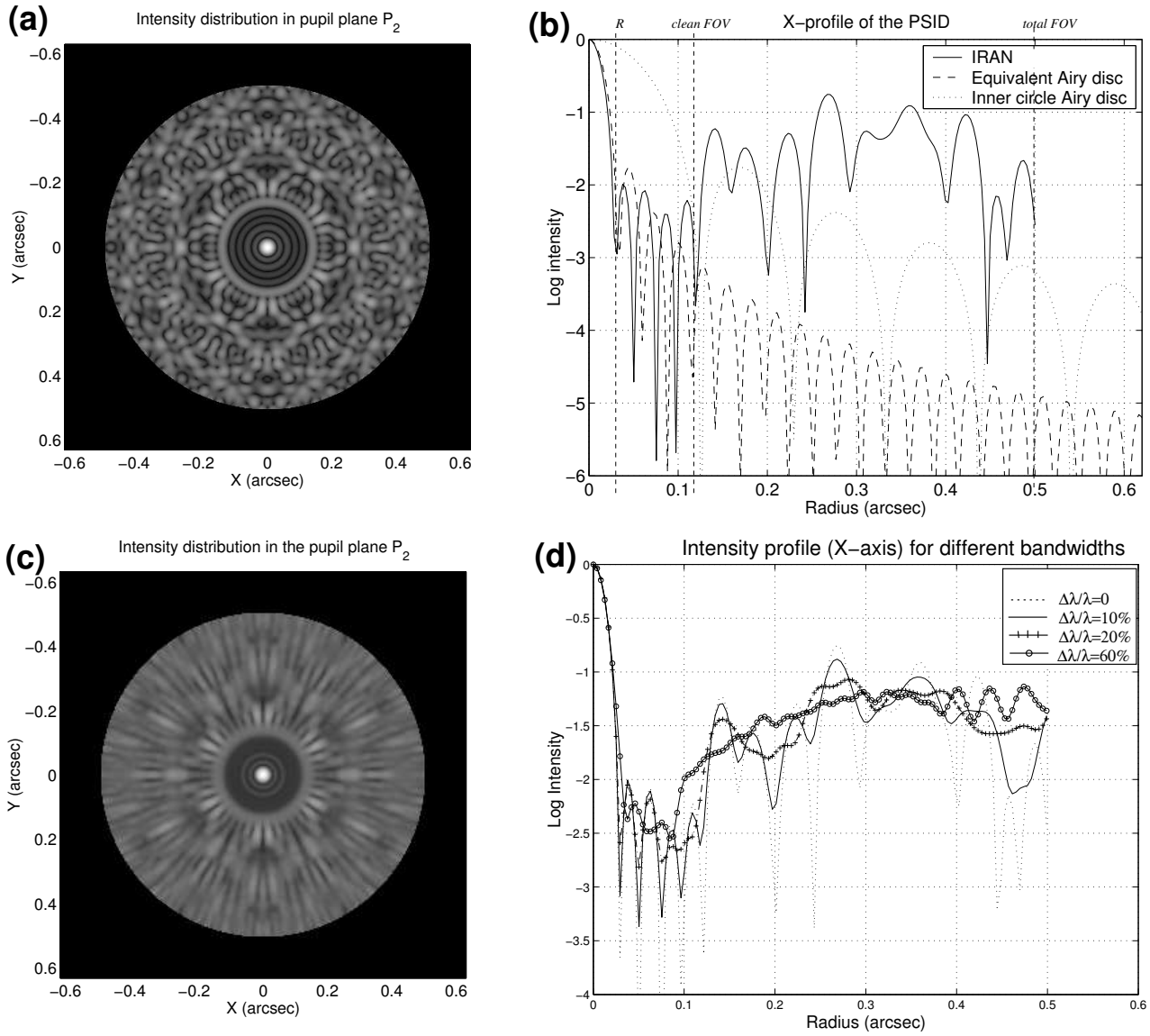

Figure 4. Simulation of the intensity pattern $I_2(\vec{r})$ (PSID), in the pupil plane P_2 for an interferometer with $N = 39$ telescopes observing an on-axis point-source. Contrast has been reduced to show weak structures surronding the central spot. The wavelength is $\lambda = 10\,\mu$m. Experimental configuration is described in the text. A pseudo Airy disc is visible at the center of the pupil image. Axis units have been converted into arcsec according to eq. 5. Pictures (a) and (b) corresponds to the monochromatic PSID and its radial cut. This cut is compared to that of the Airy disc from a single dish monolithic telescope: dashed line is for an aperture diameter D_3 (the outer circle of telescopes), dotted line is for an aperture diameter D_1 (inner circles of telescopes). Vertical dashed lines give the interferometer resolution R, the clean FOV and the total FOV. It can be noticed that the speckle-like features in the dirty zone have rather strong intensities. For that particular simulation, the energy inside the clean FOV is only 4% of total energy in the image. Pictures (c) and (d) correspond to the polychromatic PSID with central wavelength of 10μm. Bandwidth is $\Delta\lambda = 2\mu$m for picture (c).

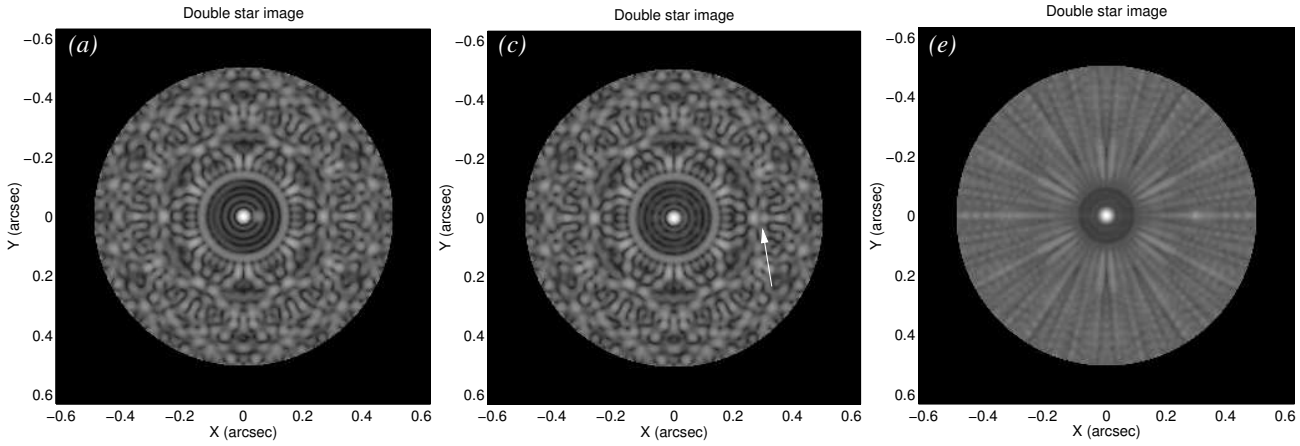

Figure 5. Simulation of the direct image of binary systems in the pupil plane P_2. The instrumental configuration is described in the text. Interferometer resolution is 30 mas. (a) monochromatic image of a binary star separated by 50 mas, with a magnitude difference of 3 at a wavelength of 10 μm. (c) monochromatic image ($\lambda = 10\mu$m) of a binary star of separation 300 mas and a magnitude difference of 3. The companion is depicted by an arrow. (e) polychromatic image ($\lambda = 10\mu$m, $\Delta\lambda/\lambda = 60\%$) of a binary of separation 300 mas and a magnitude difference of 3.

As for the on-axis case, the term $|P(\vec{r})|^2$ is a geometrical limitation of the field in the pupil plane. Within this field, the function $I_2(\vec{r})$ satisfies the property of translation invariance. Therefore, as written hereafter, a pseudo-convolution relation will exist between the source and its image.

This is a fundamental difference with the Labeyrie/Michelson pupil-densified concept,[8] where the fringes in the interferometric plane are shaped by an enveloppe which shifts when the star moves away from the optical axis. In this case both structures (fringes and enveloppe) moves at a different speed. No convolution relation exists, unless the size of the object is small compared to the individual Airy discs of the telescope (in that case the enveloppe will not move and the two recombinations are equivalent).

2.4. Object-image relation

Following the formalism of (Vakili et al., 2004),[16] we now consider the general case of on object of brightness distribution $O(\vec{\zeta})$. The object-image relation writes as the pseudo-convolution:

$$I_2(\vec{r}) = \left(\frac{\eta}{\chi}\right)^2 |P(\vec{r})|^2 \ [I_0(\vec{r}) * 0(\eta\vec{r})] \tag{5}$$

Inside the boundaries delimited by the pupil function $|P(\vec{r})|^2$, we find the classical convolution relation between the PSID and the object scaled by the factor η. This factor allows to convert a position x in meters in the focal plane into an angle $\zeta = \eta x$ in radian on the sky.

3. DIRECT IMAGES OF STELLAR COMPANIONS WITH APODIZED PUPIL

The object-image convolution relation of Eq. 5 is an interesting property for imagery at the interferometer resolution. In the simple case of a double star, the focal image is the sum of two PSIDs at a distance corresponding to the star and its companion separation times the magnification factor and weighted by their intensity ratio.

Figure 5 shows a numerical simulation of a double star image with an angular separation of 50 mas and 300 mas and a magnitude difference of 3 for monochromatic and polychromatic case. Both figure exhibit the sum of two identical, weighted and shifted structures inside the boundaries of the pupil function. Increasing the bandwidth is interesting for large binaries since the dispersion of the pseudo-speckles in the dirty field turns out to smooth their noise.

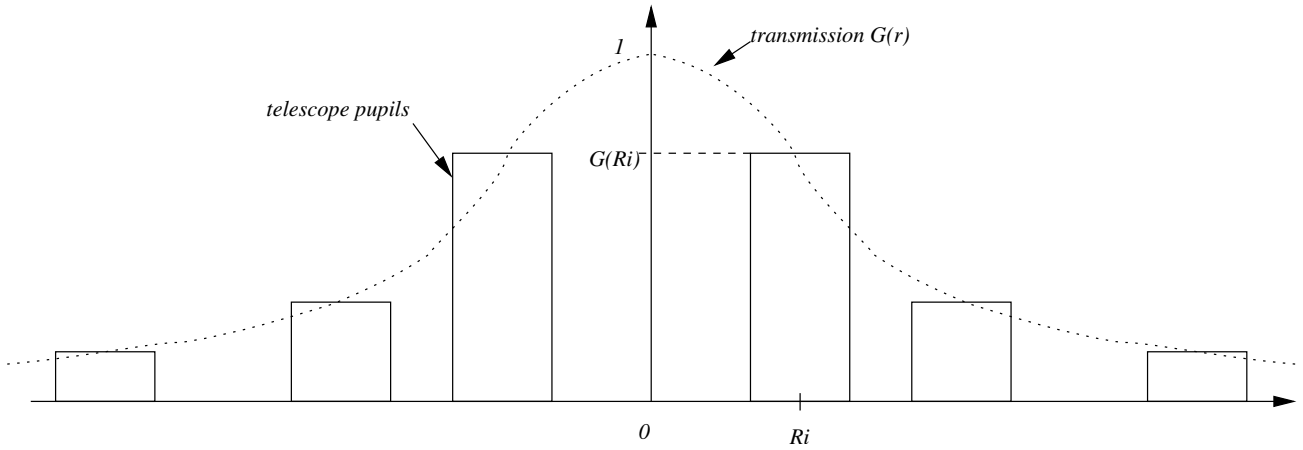

Figure 6. Principe of diluted pupil apodization. $G(r)$ is the transmission function of the equivalent single-dish apodized pupil. Individual telescopes located at positions $\vec{R}_i$ sample this function: they are given a transmission $G(R_i)$.

For close companions, an apodization technique has been tested. The principle is described on fig. 6. The interferometer is ideally equivalent to a giant monolithic telescope of diameter D_3 (the third ring). A standard pupil apodization consist in multiplying the tramsmission on the pupil by a function $G(r)$ which tends towards zero with distance to center. This technique reduces the discontinuity at the pupil edges and the Airy rings surrounding the central spot of the PSF. As the giant pupil is sampled by the telescope array, apodization can be performed by multiplying each telescope transmission by $G(R_i)$. If the number of telescopes increase, this would tend towards a giant apodized pupil with transmission $G(r)$. Although the best apodizations for circular pupil seems to be prolate circular functions,[14] we used a simple circular Gaussian to start our simulations. For a telescope located at position $\vec{R}_i$ on the ground, the transmission that we applied is

$$G(R_i) = \exp -\frac{R_i^2}{2\sigma_a^2} \tag{6}$$

where σ_a is the standard deviation taken as a multiple of the radius $D_3/2$ of the third ring of our telescope array. Experimentally this apodization can be done by inserting neutral densities in the afocal beams. Note that this corresponds to a transmission uniform over each telescope pupil; this is not really a perfect sampling of the apodization function $G(r)$ of the giant pupil.

A simulation is presented on fig. 7 for a value of $\sigma_a = 1.4D_3$ (that corresponds to transmissions equal to 0.94, 0.69 and 0.40 for telescopes on the 1st, 2nd and 3rd ring respectively). It can be seen that the apodization has an effect essentially in the clean zone of the PSID where secondary ring extinctions of the order of 90% can be attained. External speckle-like structures are not reduced. As usual, the cost is a degradation of the resolution of the interferometer (the central spot is larger). Two images of a close double star with high magnitude difference are shown on the same figure, for apodized and unapodized pupils. Direct detectability is enhanced; this is encouraging, the next step may be to apply a prolate transmission function to the telescope pupils.

4. DECONVOLUTION

A deconvolution algorithm based on likelihood maximisation has been implemented to invert the object image relation (eq. 5) and reconstruct the observed object (denoted by x in this paragraph) from its image (y) and an estimation of the PSID (made for example on a nearby reference star). The PSID is a truncated (or partially hidden) image of the PSF h (h is the function I_0 in eq. 5).

The signal restoration problem consists in the reconstruction of the best estimate x from the knowledge of a blurred signal y contaminated by noise. In our case we consider a photon noise process. The transformation suffered by x is described by a convolution which can be written as:

$$\tilde{y}(r,s) = B \ \times \ [h(r,s) * x(r,s)] \tag{7}$$

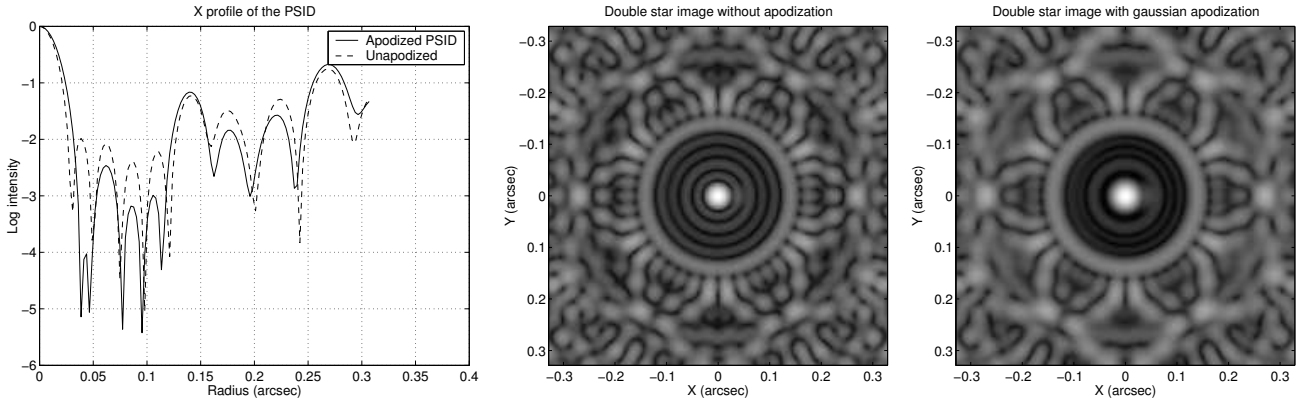

Figure 7. Simulation of double star imaging with apodization. Left: comparison between unapodized and apodized monochromatic PSID with gaussian function of width $2\sigma_a = 2.8D_3$ (see text). Middle and right: double star images with apodized and unapodized pupils. Double star separation is 40 mas (interferometer resolution is 27 mas), magnitude difference is 5. A zoom has been made on the central part of the figure.

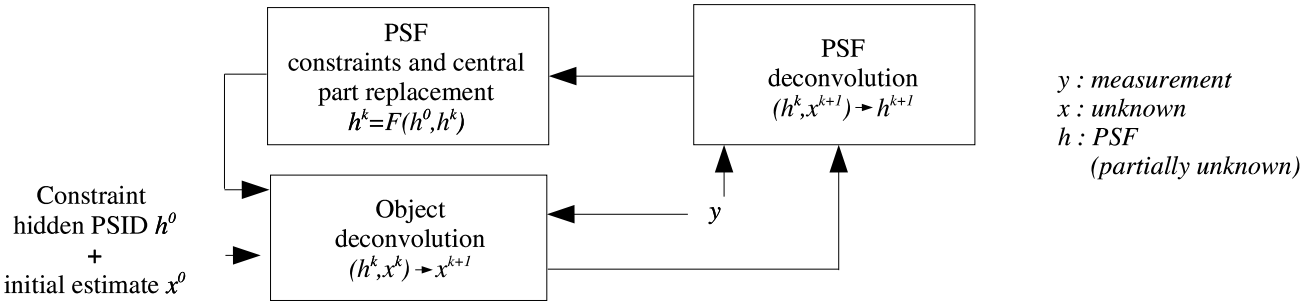

Figure 8. Schematic representation of the iterative deconvolution algorithm. Both the unknown object and the hidden part of the PSF era reconstructed by the algorithm.

with $\iint h(r,s)drds = 1$ (PSF is supposed to be normalised). where $\tilde{y}(r,s)$ is the noiseless blurred signal, h the PSF, x the object and B the circular mask (pupil function). It is important to note that part of the signal is hidden after the convolution. For example if the object is an unresolved star we only have the PSID estimate $B \times h$ and the complete PSF h cannot be obtained. This is one of the main difficulties of this inversion problem; in particular classical algorithms such as Richardson-Lucy do not apply to this case.

For a photon noise process, the intensity in the pixel i is a random variable which follows a Poisson law with mean $B_i \times [h * x]_i$. The likelihood expresses as:

$$L(x) = p(y|x) = \prod_i \frac{(B_i \times [h * x]_i)^{y_i}}{y_i!} \exp -(B_i \times [h * x]_i) \tag{8}$$

The deconvolution algorithm is deduced from the split gradient method SGM.[10] The application to our problem gives the multiplicative iterative algorithm:

$$\hat{x}_i^{(k+1)} = m_i + (x_i^{(k)} - m_i) \left[\frac{h(-r,-s) * \frac{y}{h(r,s)*x^{(k)}} + \epsilon}{h(-r,-s) * B + \epsilon} \right]_i \tag{9}$$

where m_i is the sky background and ϵ a small value used to avoid a division by zero. After each iteration a constraint on the total intensity (due to the PSF normalisation) is applied to $\hat{x}_i^{(k+1)}$ to obtain the $(k+1)$ estimate $x_i^{(k+1)}$

The first test we performed made use of the complete PSF h (inaccessible in real observations). It appeared that the results were far better than those obtained with the partially hidden PSID $B \times h$. Therefore we modified

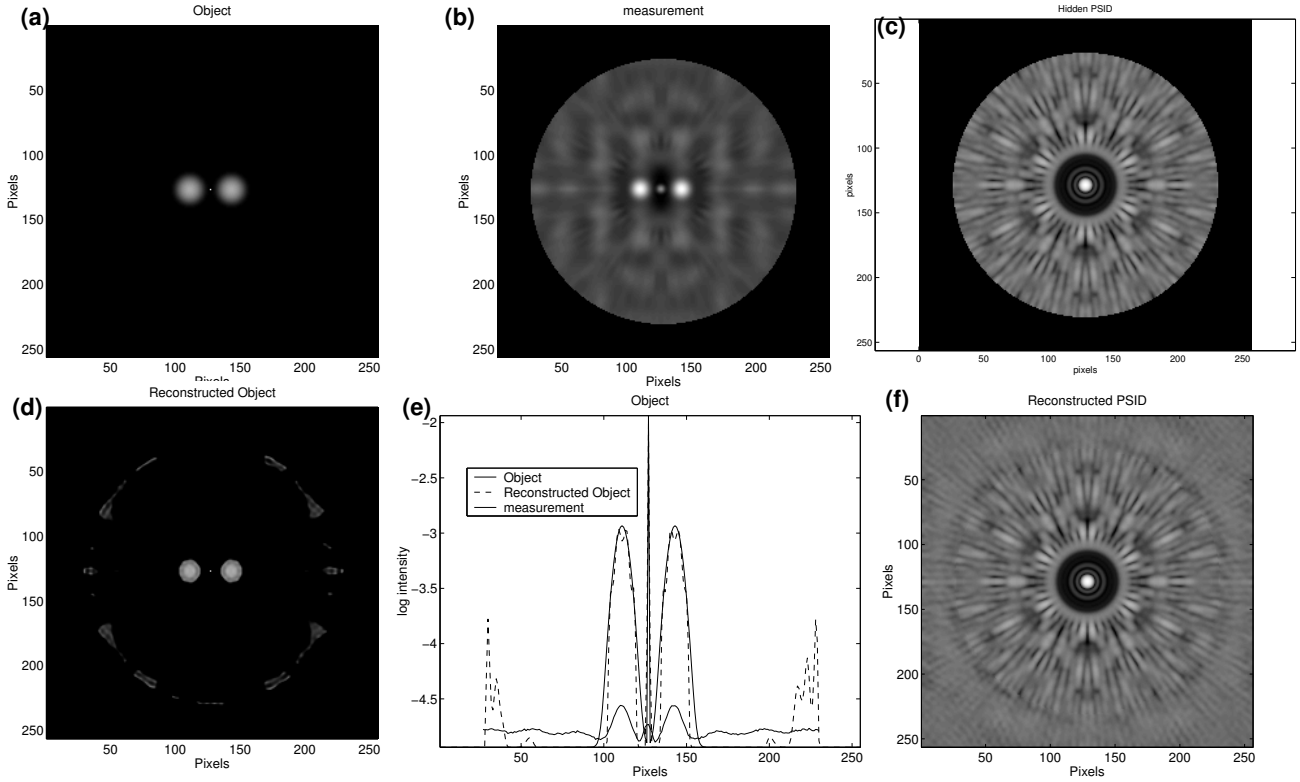

Figure 9. Result of deconvolution. (a): object; (b): observed blurred image with $N = 10^{10}$ photons (N magnitude $\simeq 6$ for 1m telescopes and 20 s exposure time). (c): PSID (truncated PSF), supposed estimated on a close reference star. (d): result of the deconvolution of the object; (e) is a comparison of the object and the deconvolution result. (f) is the reconstructed PSF.

the algorithm to allow the reconstruction of the hidden part of the PSF as well as the object. This reconstruction takes advantage of the fact that the Fourier transform of h is spatially bounded (it is indeed the autocorrelation function of the intererferometer diluted pupil function). We used this constraint to extend the PSID and we applied to it a threshold to avoid values which are too small. We can then propose an algorithmic structure, represented on figure 8, analogous to that proposed before[1,9] for blind deconvolution with, in our case a very strong constraint on the PSF.

Preliminary results are presented in fig. 9. The test object is a centered Dirac delta impulse (point-source) surrounded by two symmetric gaussians. The intensity ratio between the central point-source and the gaussians is 10. Object's size is slightly larger than the clean FOV. The simulation is made at high-light level, number of photons in the estimated object and PSID is set to a value around 10^{10}. The central wavelength is 10μm and the bandwith is 2μm. Experimental interferometer configuration is the same than above.

The best reconstruction is attained after about 50 000 iterations. Smooth structures like the two gaussians are well reconstructed with a few iterations. The central point-source needs further processing. In the reconstructed object, the intensity ratio between the central Dirac and the gaussians is 8.8 (10 in the test object). We also notice the presence of a faint (intensity is 1.5% of the maximum) ghost ring at the cutoff location of the PSID. Further tests are currently being performed on the algorithm.

5. NULLING

Detecting very faint companions around a star becomes an optical challenge with the increasing magnitude difference. For a ExPN such as 51 Pegb this difference is of the order of 7 in N-Band. Various coronographic techniques have been proposed ([14] and references therein) to reject the energy of the on-axis star. The Achromatic

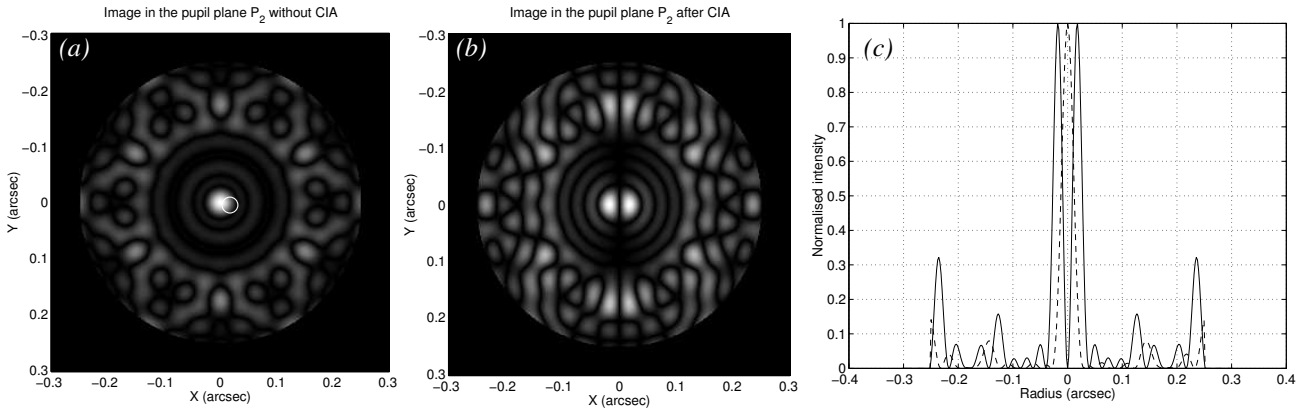

Figure 10. Simulation of double stars monochromatic images ($\lambda = 10\mu$m) in the pupil plane with and without coronography. (a) gray-level plot of the intensity without AIC for a magnitude difference of 5 and a separation of 10 mas (1/3 of the intererometer resolution). The companion (not visible) is depicted by the white circle. (b) the same with AIC. (c) intensity profiles along the x-axis (solid line is with AIC, dotted line is without, maximum scaled to 1 for both curves).

Interfero Coronograph (AIC)[6] appears as particularly suitable for ExPN detection with the IRAN interferometric configuration. Total nulling of the light incoming from an on-axis source can be achieved if the complex amplitude is a pair function of space, i.e. for a symmetric telescopes configuration.

A numerical simulation has been performed in monochromatic light with a symmetric telescope configuration composed of 36 apertures spread over 3 rings (as in the previous section). We put 6 equally-spaced telescopes on the first ring, 12 on the second and 18 on the outer ring. The external diameter is 76 m, the wavelength is 10 μm. Corresponding image plane P_1 displays a set of 36 Airy discs with the same geometry: in particular the complex amplitude is a pair function. In that case, for a perfect wavefront the nulling effect is total.

Double star simulations are shown in Fig. 10 for two different separations between the components: a small separation of 10 mas (to be compared to the interferometer resolution of 30 mas) and a large separation of 200 mas where the companion falls inside the "dirty" zone of the main star's image. It can be seen that in both cases the secondary companion can be easily detected. Note that for this simulation the magnitude difference is chosen to be 5, but since the on axis star is fully nulled one would detect ExPNs for any magnitude difference for a perfect wavefront through the whole atmosphere and interferometer+AIC -coronagraph optics. Therefore technical set-up and atmospherical conditions will be the only limitation to our proposed nulling concept. A study of the AIC performances can be found in the litterature.[2,3]

6. DISCUSSION

The advantage of using a diluted array over a large monolithic mirror, assuming the primary telescopes were mobile across the interferometric array (like the VLA radio interferometer), is that the angular resolution of the interferometric array could be adaptively changed to match the angular separation of a star and its companion. A Fizeau-type is not however optimum in terms of sensitivity because the coherent energy dilutes among more and more fringes with expanding baselines. The alternative pairwise beam-combination is on the other hand inefficient when a very large number of sub-apertures were to be recombined. All-in-one combination of a large number of sub-pupils using IRAN approach is attractive because the coherent energy concentrates in almost one pixel. Since the convolution relation subsists across the output stacked pupils any extended object will produce a one-to-one image inside that pupil, also optimum in terms of read-out and background noise. The shortcoming of IRAN however is that for imaging applications only a small central "clean-field" can be straightforwardly used. Even in this case deconvolution techniques could be applied to get rid of side-lobe noise.

In this paper we suggested a beam combination (IRAN^b) which is somewhat different from the previous concept (IRAN^a)[16] although the same goal (recombination in the pupil plane) is fulfilled in both cases and equations are almost the same. IRAN^a recombinor forms individual images falling from the telescopes onto a

pyramidal N-faces mirror. As the spatial extension on an Airy disc in in theory infinite, all images will be truncated by the edges of the mirror. This trucation is not the same for all the telescopes. The effect becomes mainly noticeable when Airy discs and mirrors have comparable size. In that case, the pupil images are degraded and object-image convolution relation breakdowns for objects larger than the Airy size of the telescope. This problem does not appear in IRAN^b, but the surfacing of a N-face pyramidal mirror giving small tilts may be a technological problem. The comparison between the two concepts have to be studied closely in details but are beyond the scope of the present paper.

The fact that IRAN produces a pseudo-Airy pattern inside the output stacked pupil arises the problem of central obscuration of the secondary mirror in a classical Cassegrain-coudé set-up of the telescopes. Thus the central zone of IRAN's field of view is "blind" to the on axis component of the source which is imaged by the interferometer. Off-axis primary telescope mirror combinations would therefore be preferable to apply IRAN, a solution which is also desirable for thermal IR interferometry to minimize background optics emission.

7. CONCLUSION

We have presented a beam-combination technique with remarkable imaging properties for high dynamic imaging with diluted optical arrays. By construction the densified image and stacked-remapping technique from IRAN can be naturally combined with the Achromatic Interfero-Coronagraph,[6] particularly suitable for coronographic imaging and detection of ExPNs compared to Labeyrie's densified pupil.

A number of questions remain open: the optimal beam combination, the effect of degrading co-phasing on the IRAN focal image, the formal definition of coronographic and/or nulling imaging of extended sources with IRAN. The fore-coming studies and results will hopefully contribute to select the best beam-combination of next generation imaging optical arrays like the VLTI or extension of already opertaing imaging arrays like NPOI. However such arrays have not been originally designed for densified imaging since their PSF exhibits strong secondary interference maxima due to their sparse and irregular input array configuration. It is therefore mandatory that future synthesis arrays with a large number of primary telescopes such as the proposed antarctic intererometer KEOPS[15, 17] involve an input baseline geometry which optimizes the PSID for its application to imaging/nulling schemes such as our proposed method.

8. ACKNOWLEDGMENTS

L. Abe benefits from a CNES post-doctoral fellowship and LUAN is supported by CNRS and UNSA.

REFERENCES

1. Ayers G.R., Dainty J.C., 1988, Opt. Let. 13, 547
2. Baudoz P., Rabbia Y., Gay J., 2000a, A&AS 141, 319
3. Baudoz P., Rabbia Y., Gay J., Burg R., Petro L., Bely P., Fleury B., Madec P.-Y., Charbonnier F., 2000b, A&AS 145, 341
4. Bracewell R. N., 1978, Nature 274, 780
5. Chelli A., Mariotti J.-M. 1986, A&A, 157, 372C
6. Gay J., Rabbia Y., 1996, C.R. Acad. Sci. Paris, 322 Série IIb, 265
7. Gillet, S., Riaud, P., Lardière O., Dejonghe J., Schmitt J., Arnold L., Boccaletti A., Horville D., Labeyrie, A., 2003, A&A 400, 393
8. Labeyrie A., 1996, A&A Suppl. 118, 517
9. Lantéri H., Aime C., Beaumont H., Gaucherel P., 1994, SPIE proc 2312, 182
10. Lantéri H., Roche M., Gaucherel P., Aime C., 2002, Signal Processing, 82, 1481
11. Mariotti J.-M., Coudé du Foresto V., Perrin G., Zhao P., Léna P., 1996, A&AS. 116, 381
12. Michelson A. A., 1920, ApJ 51, 257
13. Rousselet-Perraut K., Mourard D., Vakili F., 1997, Optical Engineering 36, 980
14. Soummer R., Aime C. Falloon P. E., 2003, A&A 397, 1161

15. Vakili, F., Aristidi, E., et al., SF2A-2003, Eds.: F. Combes, D. Barret and T. Contini. EdP-Sciences, Conference Series, p. 365.
16. Vakili, F., Aristidi, E., Abe L., Lopez B., 2004, A&A Suppl., in press
17. Vakili, F., Aristidi, E., Fossat E., Abe L., Agabi A., Belu A., Lopez B., Domiciano A., 2004, this conf.